# Use of 1D [Pr(BTC)(H₂O)₆] MOF as a Filler for Fabrication of Matrimid® based MMMs

[1]Asma R. Tariq[*], [1]Misbah Sultan[**], [1]Tariq Mahmud[***], [2]Ghayoor Abbas Chotana,
[3]Muhammad Rizwan Dilshad, [4]Asim Laeeq Khan, [1]Muhammad Imran,
[5]Saadia Rashid Tariq and [6]Prof. Dr. Klaus Müller-Buschbaum

[1]*School of Chemistry, University of the Punjab, P.O. Box 54590, Lahore, Pakistan.*

[2]*Department of Chemistry, Syed Babar Ali School of Science & Engineering (SBASSE), Lahore University of Management Sciences (LUMS), Sector U, DHA, Lahore Cantt. 54792, Pakistan.*

[3]*Institute of Engineering and Technology, University of the Punjab, P.O. Box  54590, Lahore, Pakistan.*

[4]*Department of Chemical Engineering, COMSATS University Islamabad, Lahore Campus, Defence Road, Off Raiwind Road Lahore, Pakistan.*

[5]*Department of Chemistry, Lahore College for Women University, Lahore, Pakistan.*

[6] *Institut für Anorganische und Analytische Chemie, Justus-Liebig-Universität Gießen, Heinrich-Buff- Ring 17, 35392 Gießen, Germany. (Previously affiliated with; Facultät fur Chemie und Pharmazie, Anorganishe Chemie, Julius-Maximilians-Universität Würzburg).*

tariqrasma@gmail.com*, misbahsultan@ymail.com**, tariqm06@yahoo.co.uk***

**Summary:** Selection of good filler-polymer pair results in improved gas separation performances. Present study deals with fabrication of Matrimid based hybrid or mixed matrix membranes (MMMs) by using three weight loadings (10, 20 and 30 wt. %) of 1D rod shaped nanoporous [Pr(BTC)(H₂O)₆] metal organic framework (MOF). The fourier transform infrared (FTIR) spectrophotometric analysis indicated the bonding of lanthanide metal ion with the linker and thus formation of the MOF, and further revealed that the structure of MOF remained intact after incorporation into the polymer matrix. Powder X-ray (PXRD) analysis revealed purity and crystallinity of the MOF while the PXRD results for the MMMs indicated that crystallinity of the MOF remained unaffected after fabrication of the MMMs. The Scanning electron microscopy (SEM) results gave an indication of the formation of the MOF in same morphology as it is previously reported. Additionally, nice distribution and well adherence of the additive particles throughout the polymer matrix was observed while the interfacial voids were visibly absent. The MOF and the MMMs were thermally stable and crystallinity of MOF particles remained intact after dispersion into polymer matrix. The Brunauer Emmett Teller (BET) surface area of the MOF was also obtained that indicated its permanent porosity. The prepared MMMs were flexible enough to handle for all analysis. These findings led to conclude that a proper polymer-filler pair was made that produced defect free MMMs. The prepared MMMs can be evaluated in future for their performance towards separation of different gases after modification of the pore of the filler.

**Key words:** 1D [Pr(BTC)(H₂O)₆] nanoporous MOF- Matrimid-MMMs, FTIR, PXRD, SEM, BET surface analysis.

## Introduction

There is an immense increase in worldwide annual $CO_2$ and $CH_4$ gas emission due to combustion of fossil, industrialization and increasing population [1]. The GHGs are the major contributor to global warming [2, 3]. IPCC predicts that a rise in $CO_2$ concentration level in the atmosphere is suspected up to 570 ppm until 2100. This rise may cause rise in the earth surface temperature by 1.9°C and sea level by 3.8 m. [4, 5]. The carbon capture utilization and storage (CCUS) can be used to control this discharge but high cost is linked with the capture step. Likewise, the undesired impurities for example hydrogen sulfide and $N_2$ etc. present within the natural gas diminish its quality and causes corrosion of

the process units in addition to causing environmental problems [6, 7]. The large energy deficit associated with the conventional cryogenic distillation [8], use of activated carbon (AC), carbon molecular sieves (CMS) and amine based wet scrubbing [9] has attracted the scientists towards the energy efficient, environment friendly and cost effective membrane technology for gas separation processes [10].

Both the inorganic membranes and polymeric ones, offer wide spread use in numerous industrial applications for example microfiltration, water purification, reverse osmosis (RO), desalinatioin,

---

[*]**To whom all correspondence should be addressed.**

hemodialysis, heavy metal removal, and gas separation etc. Particularly for gas separation, the selectivity coefficients and permeance are the key features that define the aptness and efficiency of membranes for a specific process [6, 11, 12]. Additionally, the electrical conductivity, thermal resistance, porosity and swelling must also be optimized at the same time [13, 14].

Inorganic membranes are characterized by greater chemical, thermal, and mechanical stability as well as long-term durability while their textural features are found to be responsible for improved permeability of gases in comparison to the polymeric membranes [15]. Contrarily, the brittleness, processability, cost, scale-up potential and defects of inorganic membranes are known factors that limit their commercialization [16, 17].

The polymeric membranes offer excellent stability, ease of operation, improved efficiency and low energy requirement [6] and thus find enormous application in the field of separation.

Polysulfone (PSf), PBI, cellulose acetate (CA), polyethersulfone (PES) and polyimide (PI) were immensely studied in the field of gas separation as they are capable to form defect-free membranes possessing cross-linking ability and high mechanical strength [18, 19]. Such glassy polymers offer high free volume but the filler particles get less remarkably adhere to them [20]. In addition, the harsh conditions of high $CO_2$ concentration and feed pressure cause plasticization effect in these glassy polymers which results in compromised selectivity and permeability. Further, the elevated temperatures result in structure instability and fouling of these glassy polymers. All the above mentioned aspects showcase the restricted commercialized use of such thin membranes for the purpose of $CO_2$ separation [21]. The commercial use of these polymeric membranes for the separation and/or storage of the $CH_4$ & $CO_2$, can be realized if such membranes execute a smaller impact on environment in addition to their cost efficiency while these should also be well efficient to surpass the quantified selectivity-permeability trade-off [22-24]. Considering these effects, it can be understood that the glassy polymer membranes should characteristically exhibit high selectivity and reduced permeability, as compared to the rubbery polymeric membranes which execute a trend entirely opposite to that of the glassy polymers [25].

Separation efficiency of the conventional polymer membranes can be upsurge with the addition of suitable inorganic filler with permanent porosity however their processing ease and cost should be economic from their industrialization view point as compared with fabrication of inorganic membranes [26]. The fabrication of such hybrid or mixed matrix membranes (MMMs) resulted in evolution of the development of the gas separation processes which thus presented a promising alternative to the pure polymer membranes [27]. A combination of the gas separation properties of the porous filler materials and the best suited mechanical properties coupled with the economical processability of the polymer matrix are used to design efficient gas separation modules [27]. The development of MMMs are considered to be a sustainable solution to drawbacks of the conventional separation processes for example thermal swing adsorption, pressure swing adsorption, cryogenic distillation, etc. [27].

Polysulfone (PSf) is a widely used glassy polymer that is chemically and thermally stable thermoplastic polymer. Where the sulfone aryl and ether groups constitute the backbone repeat units. PSf is one of the largely used polymer for the gas separation applications due to its easy processability, excellent gas permeability and selectivity performances [28].

Use of PSf is previously reported such as in zeolite composite membranes [29] while fabrication of ZIF-8/Matrimid® MMMs offers extra polymer free volume [30]. Moreover, optimal concentration (30 wt.%) of ZIF-8 into the glassy Matrimid® polymer is also used previously [31]. Polyoxometalates (POMs) encapsulation for formation of their MMMs with PSf is also reported recently [32].

Novel PSF composite ultrafiltration membranes were fabricated with low concentration of polydopamine-functionalized graphene oxide particles that showed high flux as well as fouling resistance [33].

While gas separation efficiencies for $O_2$, $CO_2$ and $N_2$ are also reported to be evaluated using flat MMMs incorporating 5, 10, and 20 wt. % loadings of MCM-41 and amino functionalized silica. The obtained MMMs executed improved permeabilities for $O_2$ (in the range of 1.2 and 1.7 Barrer) and $CO_2$ (in the range of 4.2 & 8.1 Barrer) in comparison with the pristine PSf module (0.8 Barrer). However, the compromised selectivity value was obtained for the $CO_2/N_2$ (between 25 & 41 %) and $O_2/N_2$ (between 6 & 8 %) gas pairs. This decrease was however insignificant in comparison with the neat modules (8 & 39 %, correspondingly). Additionally, the size differences between the $CO_2$ and $N_2$ gas molecules as well as the increased solubility of $CO_2$ due to its condensability have made MCM-41/PSF MMMs to be comparatively selective for the $CO_2/N_2$ pair than the $O_2/N_2$ gas mixture. Introduction of amino groups caused stronger interactions with the MCM-41-$NH_2$/PSF MMMs that resulted in improved selectivity for the both

gas pairs in comparison with the un-functionalized MCM-41/PSF modules [27].

Ding *et al*. incorporated KIT-6 silica into PSF with 0-8 wt.% concentration of additive. PSf matrix embedded with 2 wt.% of KIT-6 produced MMMs that were free of voids. Increase of wt.% concentration of KIT-6 from 0 to 2 in the MMMs caused ~48 % increase in the $CO_2$ permeability while the ideal selectivity of $CO_2/CH_4$ gas pair remained almost unchanged. However, further increase from 2 wt. % loadings of KIT-6 in to the PSf matrix resulted in creation of voids in the MMMs that in turn improved the $CO_2$ gas permeability at the cost of ideal $CO_2/CH_4$ selectivity. Yet, the controlled KIT-6 loadings proved it to be a potential additive for the PSf matrix for gas permeation [34].

Kim and Marrand reported increased $CO_2$ permeability (by 275 %) of 40 wt.%-MCM-41/PSf MMM as compared with bare PSF [35]. Similarly, Jomekian *et al*. reported ~193 % boost in $CO_2$ permeability over the bare PSF module upon use of MCM-48 as a filler for the development of PSf based MMMs [36].

The MOFs are potential candidates for applications like gas separation as they hold regular microporosity and tunable surface chemical properties at their molecular level [37, 38].

Guo *et al*. reported fabrication of PSf based thermally stable MMMs using varying concentration of $NH_2$-MIL125(Ti) between 10 and 30 wt.%. The MMM with 30 wt. % concentration executed the highest $CO_2$ permeability (40 barrer) and the 20 wt.% module executed the maximum $CO_2/CH_4$ selectivity of 29.5 respectively [39].

Similarly, the silica (MSS)/ZIF-8 composite/PSf MMMs also exhibited better gas permeability due to their high micro-mesoporosity. However, increase in concentration of additive even up to 32 wt.% did not cause momentous change in selectivity [40, 41]. However, Ordoñez *et al*. reported improved $O_2/N_2$ and $H_2/CH_4$ separations (8.3 and 118 respectively) due to increased free volume offered in the ZIF-8/PSf MMM [30]. Moreover, MMMs using PSf as polymer phase incorporated with the ZIF-8, HKUST-1, Silicate-1 and the mixture of Silicate-1 and MOF exhibited enhanced permeability but compromised selectivity for the $CO_2$ and $CH_4$ gas pair [42]. Zornoza *et al*. reported improvement in the separation factor of the hybrid membranes obtained by addition of $NH_2$-MIL-53(Al) as filler into the PSf [43]. Similarly ZIF-8 is known to increase the porosity of the P-84 membranes in the resulting MMMs [44].

Car *et al*. reported compromised $CO_2/CH_4$ ideal selectivities for PSF based MMMs loaded with 10 wt.% $Mn(HCOO)_2$ & $Cu_3(BTC)_2$ fillers by the factors of 50 % and 58 %, in that order [45]. Rodenas *et al*. described that embedding of 25 wt.% concentration of $NH_2$-functionalized MIL-101(Al) in to the PSf matrix can enhance the $CO_2$ gas permeability as well as the $CO_2/CH_4$ separation factor in the resulting MMMs by factors of 63 % and 22 %, correspondingly [46]. High performance glassy polyimides (PI) are previously reported to execute an 84 % improvement in the ideal selectivity of $CO_2$ & $CH_4$ gas pair with an optimal 15 wt.% concentration of the MIL-53 [47]. Similarly, a 30 wt.% concentration of $Cu_3(BTC)_2$ into the Matrimid® led to a 121 % increase in $CO_2$ permeability as compared to the bare Matrimid® module without affecting the selectivity value [48].

Amine functionalization of mesoporous silica is previously known to improve permeability as well as selectivity. Likewise, the polyethylenimine-functionalized-MCM-41 executed improved $CO_2$ permeability as well as $CO_2/CH_4$ pair selectivity in comparison with the hybrid membranes embedded with un-functionalized MCM-41filler [49]. Khan *et al*. reported aminopropyltrimethoxysilane functionalized MCM-41 caused the elimination of voids in the PSf based MMMs while considerably improved $CO_2/N_2$ and $CO_2/CH_4$ selectivity values were observed [40].

Chew *et al*. described development of PSf based MMMs using (3-Aminopropyl) triethoxysilane (APTES) functionalized KIT-6 in different wt.% loadings (0-4 %). The FESEM images indicated that the MMMs casted at a decreased $NH_2$KIT-6 concentration of 0-2 wt. % were free of voids. An increment in the $CO_2$ permeability value and the ideal selectivity value for $CO_2/CH_4$ gas pair was observed upon increasing concentration of $NH_2$KIT-6 from 0 to 2 wt. % in the PSf matrix. However, a drop in the ideal selectivity value for the $CO_2$ & $CH_4$ gas pair was observed upon further increment in $NH_2$KIT-6 loading. Chew *et al*. described, optimum loading of $NH_2$-KIT-6 for the resulting MMMs to be 2 wt. % that brought substantial increase in ideal selectivity (about 47 %) of $CO_2/CH_4$ gas pair [50]. Similarly, the highly stable sulfonated UiO-66 MOFs that were functionalized with mercaptopropyl trimethoxysilane were also previously reported for the development of PSf based MMMs [51].

$^3_\infty[Sr_{0.9}Eu_{0.1}Im_2]$@Matrimid (where Im$^-$=imidazolate), $^3_\infty[Sr_{0.9}Eu_{0.1}Im_2]$@PSF, and $^2_\infty[Tb_2Cl_6(bipy)_3].2bipy$@PSF (where bipy=bipyridyl) are evidenced as luminescent MMMs [52]. $^3_\infty[Ce(Im)_3ImH].ImH$@PSF, $^3_\infty[Sr_{0.90}Eu_{0.10}(Im)_2]$@PSF, and $^3_\infty[Ba_{0.98}Eu_{0.02}(Im)_2]$@PSF luminescent MMMs

were evaluated for the progress of the humidity induced luminescence intensity quenching [53]. Likewise, Y-BTC or MOF-76(Y) is known to be exceedingly selective for $H_2$ sorption [54].

The right choice of a microporous lanthanide-metal organic framework (Ln-MOF) additive for the fabrication of MMMs may bring improvement in the selectivity as well as permeability of the resulting modules. Considering the fact that the rare earths (RE) may be employed to obtain materials with tunable properties [55] the present studies were designed so as to deal with the synthesis of 1D nanorods of [Pr(1,3,5-BTC)($H_2O$)$_6$] [56] using it for the synthesis of [Pr(BTC)($H_2O$)$_6$]/Matrimid®5218 based MMMs. The thermal and morphological properties of the resulting MMMs were then explored. The prepared MOF possessed a highly stable frame work and exhibits good surface area *viz.* 112.450 m²/g and pore width of 4.093 nm.

The 10, 20 and 30 wt. % concentrations of this MOF were used for the fabrication of PSf, Matrimid and CA based MMMs. To the best of our knowledge, this is the first investigation on use of 1D nanorods of [Pr(1,3,5-BTC)($H_2O$)$_6$] MOF as an additive in Matrimid based MMMs that can be checked for the selective separation of different gases in future after proper modification of its pore.

**Experimental**

*Materials reagents and chemicals*

High quality acid resistant, borosilicate Pyrex glass ware was used for synthesis and further experimentation. Any chances of impurities that may be adhered to the glassware used was eliminated by thorough washing with deionized (DI) water, and then with acetone. The obstinate inorganic impurities from glass apparatus were get rid of using lab prepared chromic acid. Organic impurities (if may be present) from the sample vials were removed by thorough rinsing by using acetone, Sample vials were dried in an electric oven and were then evacuated using vacuum line. The sample packing was performed in the glove box in an air free environment.

The local chemical suppliers provided us with all of the reagents and chemicals that were not further purified before use. The right selection of a suitable polymeric matrix is definitely quite significant as it has been previously discussed. So Matrimid was used as polymer matrix for the present study. Its structure is shown in Fig. 2

Marjan Polymer Industries Pakistan imported the Matrimid 5218® from Ciba Specialty Chemicals North America for the present study. The polymers were dried for 24 hours in a vacuum oven at about 120°C or at suitable temperature before use. Incorporation of fillers in it can improve the permeability of resulting MMMs. Commercial grade acetone was doubly distilled and used for final rinsing of glass apparatus. 99.9% Dichloromethane were acquired from the Sigma Aldrich. Chloroform was obtained from BDH. Distillation of commercial grade ethanol was performed to obtain absolute ethanol. Analytical Grade methanol was purchased from E Merck. 99.9% Pr($NO_3$)$_3$.6$H_2O$ (trace metal basis) and Trimesic acid (95% pure) were obtained from Sigma Aldrich.

*Methodology*

*Procedure for synthesis of MOF*

Preparation of [Pr(1,3,5-BTC)($H_2O$)$_6$] MOF was performed according to the previously published procedure however with minor modifications were made wherever necessary [56]. Accordingly, the aqueous solution of The metal salt [Pr($NO_3$)$_3$.6$H_2O$] solution with a pH=3-4 was prepared in deionized water while continuous agitation was carried on during addition of solvent. The direct precipitation of the pre-reported [Pr(1,3,5-BTC)($H_2O$)$_6$] complex having a nano-rod morphology was followed by adjusting the concentration of BTC linker and metal salt to be 4:0.5 mmole ratio on that order was prepared in de-ionized water. BTC solution was separately prepared in 1:3 ethanol-water solution to which 0.1 mL of the Pr($NO_3$)$_3$ metal salt solution was added with continuous stirring at room temperature. The addition with agitation of the metal salt into the linker immediately produced sufficient amount of white precipitates of [Pr(1,3,5-BTC)($H_2O$)$_6$]. The stirring was continued for 10 min. afterwards the precipitates were centrifuged and collected. A schematic representation for the synthesis of inorganic filler can be seen in Fig. 1. The obtained MOF precipitates were washed a number of times by using water and ethanol (40 mL) followed by air drying and vacuum drying for their characterization. The perfectly dried MOF powder was stored under Ar to protect it from air and moisture for its further use as additive in Matrimid. ATR-FTIR and Powder X-ray diffraction spectroscopic techniques were used to check its phase purity.
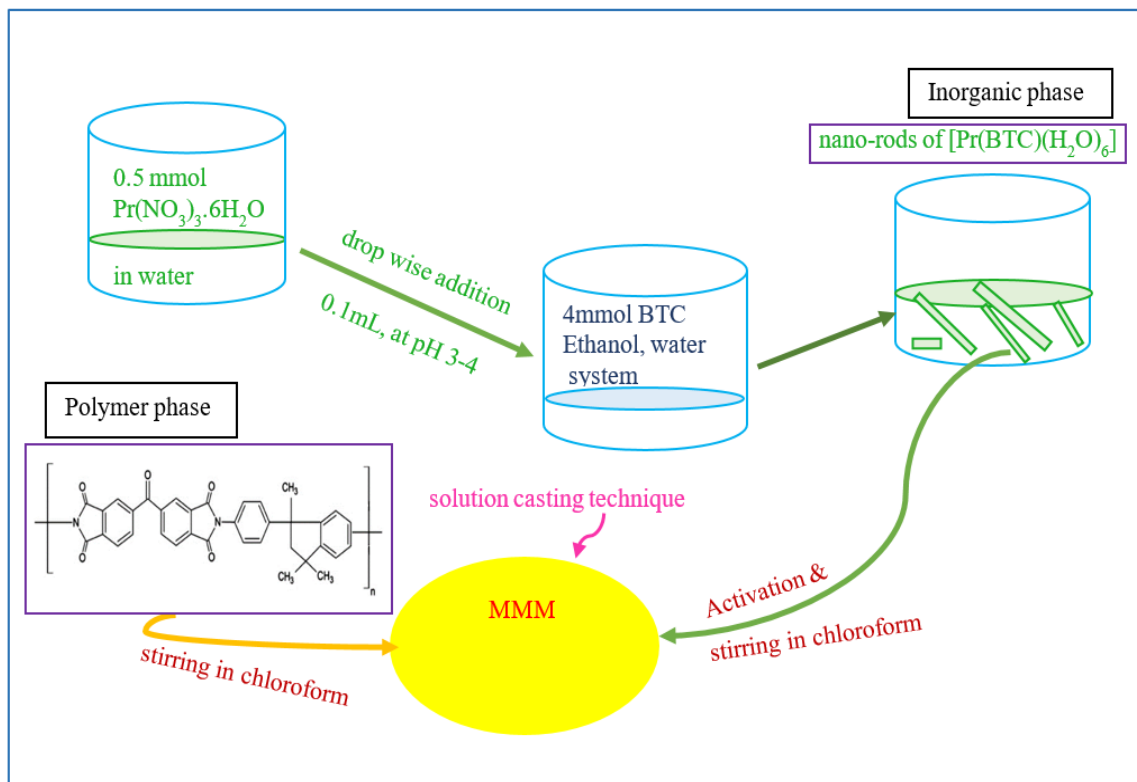
Fig. 1:   Graphical abstract representing formation of MOF and fabrication of $[Pr(BTC)(H_2O)_6]$-Matrimid MMMs through incorporation of inorganic $[Pr(BTC)(H_2O)_6]$ filler.
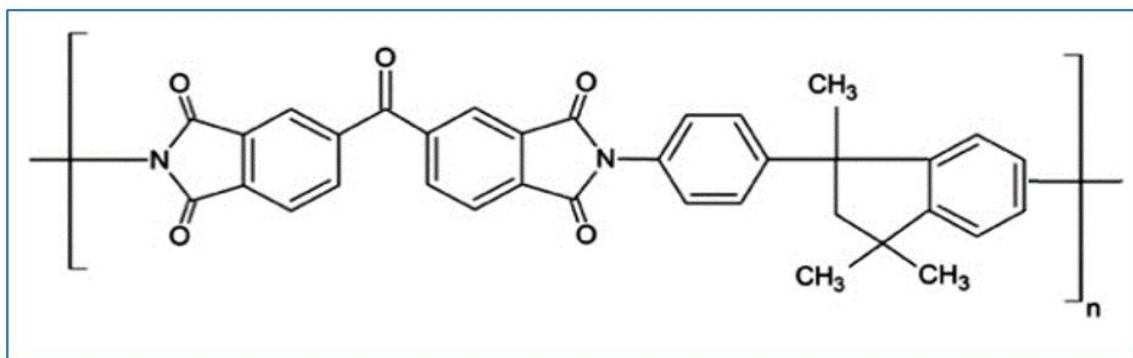


Fig. 2:   Matrimid (a polymer of 3,3',4,4'-benzophenone tetracarboxylic dianhydride and diaminophenylindane units).

*Activation of MOF sample*

This perfectly dried MOF was activated by pre-reported solvent exchange activation procedure by successive use of absolute ethanol and acetone. This solvent activation procedure was repeatedly performed followed by drying under vacuum. Afterwards the MOF powder was thermally activated by heating at 70°C for almost 36 hours [56].

*Membranes casting*

*i) Preparation of pristine polymer membranes*

The pristine polymer module was casted by using solution casting technique. The polymer was completely dried by heating at about 110°C using vacuum oven for 24 hours. Its 3.5 % solution was prepared in chloroform by taking appropriate amount followed by overnight stirring. The thus obtained

viscous solution was poured on flat bottom glass petri plate that was covered by inverted large funnel with cotton plug to control the evaporation from the medium.

*ii) Preparation and casting of the MMMs*

The finally grinded MOFs sample were embedded into the polymer matrix for three reasons: (a) in order to avoid their agglomeration, (b) to obtain a MMM with good additive distribution throughout the polymer matrix, (c) to assure enough compatibility between the selected filler phase and that of the polymer phase.

The compatibility between both phases can be improved by adopting a precise "priming protocol". Generally, polymer was dissolved in a pre-calculated volume of chloroform that was stirred continuously for 24 hours at room temperature. The 10%, 20% and 30% suspensions by weight of the activated MOF filler concentration were separately prepared by using the equation given below:

$$Filler\ loading\ (weight\ \%) = \left[\frac{wt.of\ filler}{wt.of\ polymer+wt.of\ filler}\right] \times 100$$
(1)

The separate dispersion and stirring of the prepared MOF was also carried out for almost 24 hours in the same solvent (chloroform). Almost 20 wt. % of the whole Matrimid polymer solution was converted to the separately prepared MOF suspension that was followed each time by stirring as well as sonication for about 5-10 minutes. A batch mode addition *viz.* 20 wt. % of the residual Matrimid solution in chloroform was carried out into the separately dispersed and stirred MOF suspension. A continuous agitation for almost 2 hours was performed after every batch of Matrimid solution was added that further followed a 15-20 minutes sonication. This batch wise addition was followed until it added the all polymer solution in to the MOF suspension. The addition of last batch of Matrimid solution into the stirring suspension of MOF filler was also followed by sonication for 10-15 minutes so as to avoid the agglomeration of additive particles in their greater concentration. The resulting polymer/filler suspension was cast on to a flat surfaced, 3 inches glass petri plate. This petri plate was mounted/placed on a possibly perfect balanced and flat surface at room temperature. The cast suspension was then covered by using large inverted funnel. The open end of the funnel was filled with cotton in order to control the rate of solvent evaporation. The dried membranes were removed from petri plate after 48-72 hours, and were subject to curing at about 140°C at a rate of 20°C/hour increase

in temperature. A schematic representation of the MMM casting can be seen in Fig. 1. The finally obtained membranes were kept in vacuum desiccator after appropriate labeling prior to further studies.

*Characterization*

The confirmation of the preparation of the Ln-MOF, bare polymer membrane and the well dried MMMs was carried out thorough appropriate analytical techniques such as ATR-FTIR and PXRD spectrophotometry. The MOF and their MMMs were also investigated for their thermal properties by using TGA technique. SEM was used to explore the morphological characteristics of the additive and 10 wt. % MMM [55].

The identification of structural features and particular functional groups was performed by ATR-FTIR spectrophotometer. The spectra were recorded at 64 scans/Seconds by using Agilent Cary 630 ATR-FTIR while at resolution set < 2cm$^{-1}$. The diamond crystal fitted with ATR-FTIR was best suited for most of the samples. The scanning range was 4000-400 cm$^{-1}$ and Agilent Microlab PC software available with the instrument was used to remove the back ground noise where ever it was necessary.

ATR-FTIR analysis for MOF sample required no special sample preparation. The MOF samples were only grinded to obtain fine powder that was carefully mounted on ATR-FTIR crystal to obtain the spectra containing specific identification peaks of the MOF.

A nicely cut tiny part from MMMs was obtained for their ATR-FTIR analysis and cautiously mounted on ATR-FTIR crystal to obtain their spectra containing specific identification peaks. All X-ray powder diffraction applications were made by using the desktop diffractometer, Bruker D2 Phaser in Bragg-Brentano geometry. The $2\theta$ range for the MOF and MMMs modules was in the range of 5 to 50° with maximum accuracy *viz.* ± 0.02° observed throughout the complete measuring range. The advanced 1D LYNXEYE unique detector used was absolutely faultless. This technique was used to determine the crystallinity of the samples. Cu Kα radiations (λ=1.542 Å standard ceramic sealed tube at 0.02° S$^{-1}$ scan rate) were used.

The grinding of MOF sample was performed by using small Teflon mortar and pestle. The silicon wafer slide with a thin smear of MOF spread on it was then placed in the PXRD instrument to obtain their diffractograms.

The PXRD analysis of the MMMs required no special need of sample preparation. The smaller length piece from MMMs were cut carefully with clean and dust free scissors that were used for PXRD analysis.

The accurate and concurrent measurements of weight changes were estimated through Thermal Analyzer SDT Q600 on selected samples in $N_2$ environment from room temperature to maximumly at 1000°C while its flow rate was kept to be 20 mL/minute with ramp rate of 10°C/minute.

The completely dried and annealed MOFs and their MMMs at 120°C were used for their thermal analysis.

The SEM micrographs of the additive (MOF) and its selected MMM with 10 wt. % loading were obtained through FEI Nova 450 NanoSEM on order to get a comprehension of their surface morphology at different resolutions. The sputter coating of the samples with gold particles was performed to make their surfaces conductive as well as more receptive. Resultantly, the SEM images with ultrahigh resolution can be acquired as the surface sensitivity can be delivered now at various magnifications under ideal operating conditions and also by using the both high- and low-voltage. The in-situ plasma cleaner was used to avoid any risks of hydrocarbon contamination inside the chamber.

The activated MOF sample was mounted on sample holder of Scanning Electron Microscope (SEM). The sample grinding was not performed so that the obtained morphology of the MOF may not be disturbed. It was needless to perform sample preparation for the MMM module. Only a nicely cut small portion of the MMM was used for obtaining cross sectional SEM micrograph.

## Results and Discussion

### Characterization of [Pr(BTC)(H₂O)₆]MOF

The prepared MOF was used as a filler for fabrication of Matrimid polymer in three different concentrations. The prepared MMM modules could offer possible applications for gas separation.

The FTIR spectra of the MOF was in accordance with previously published FTIR spectra [57, 58, 59]. The $H_3BTC$ ligand was deprotonated as indicated by absence of stretching vibrations at 2658, 1720 and 1676 cm$^{-1}$ (OCOOH). The lanthanide ion got associated with the carboxylate functional group as attributable by the presence of high energy, sharp and long asymmetric ($v_{as}$(C-O)) stretch that appeared at

1547.98 cm$^{-1}$ and the weak asymmetric ($v_{as}$(C-O)) stretch 1604.3 cm$^{-1}$. Moreover, the strong and long sharp peak that appeared at 1366 & 1428.48 cm$^{-1}$ was meant for the symmetric ($v_{as}$(C-O)) stretching frequency of the carboxyl groups. Additionally, these two sets of above mentioned stretchs might be described as confirmation for the presence of the dicarboxylate on the MOF structure. The FTIR spectra of [Pr(BTC)(H₂O)₆] MOF is provided in the Fig. 3a.

The PXRD pattern of MOF is shown in Fig. 3b. The $2\theta$ value *viz.* 17.1° was assigned to the maximum intensity diffractogram for this MOF. Yet, the obtained PXRD data indicated that the other impurities were absent in the sample of the activated MOF. Moreover, the narrow but sharp peaks were appeared for the MOF indicating it to be crystalline in nature [56]. Praseodymium belongs to light lanthanides group, possessing high coordination number. The monoclinic, space group *Cc* was attributed to the crystal structure of the samples. Six water molecules coordinate to the central Pr atom with their oxygen atoms while 1,3,5-BTC linkers coordinate through oxygen atoms of their three different carboxylate groups that result in a tricapped trigonal prismatic geometry.

The obtained MOF sample was suggested to be isostructural with the previously known bulk phase of the [La(1,3,5-BTC)(H₂O)₆] MOF because quite similar peaks were observed as an evidence. Further, there was a small shift in the spectra towards the large angle as Pr$^{3+}$ ion possesses smaller radius due to the phenomena of lanthanide contraction [60].

The BET surface area measurements were performed using $N_2$ at 77K. The surface area was found to be 112.450 m²/g. Pore volume was evaluated to be 0.126 cm³/g, and the pore width of 4.093 nm was calculated using DFT. The obtained surface area was found to be higher than the previously published results for isostructural [Ce (BTC)(H₂O)₆] MOF [61].

The as possibly full morphological properties of the activated [Pr(BTC)(H₂O)₆] MOF were studied by scanning electron microscopy (SEM) (Fig. 3c). The formation of 1D nano-rod like architecture of the MOF without any fantails can be observed (Fig. 3c) that was additionally found in agreement with the previously published morphological features of the same MOF [56, 62]. The act of BTC linker as soft template actually produced these individual nano-rods [56]. The varying sized 1D nano-rods of light green MOF were obtained that were crushed after activation so that a fine powder could be obtained for incorporating into the polymer matrix so the present study did not involve size measurement of these nano-rods.
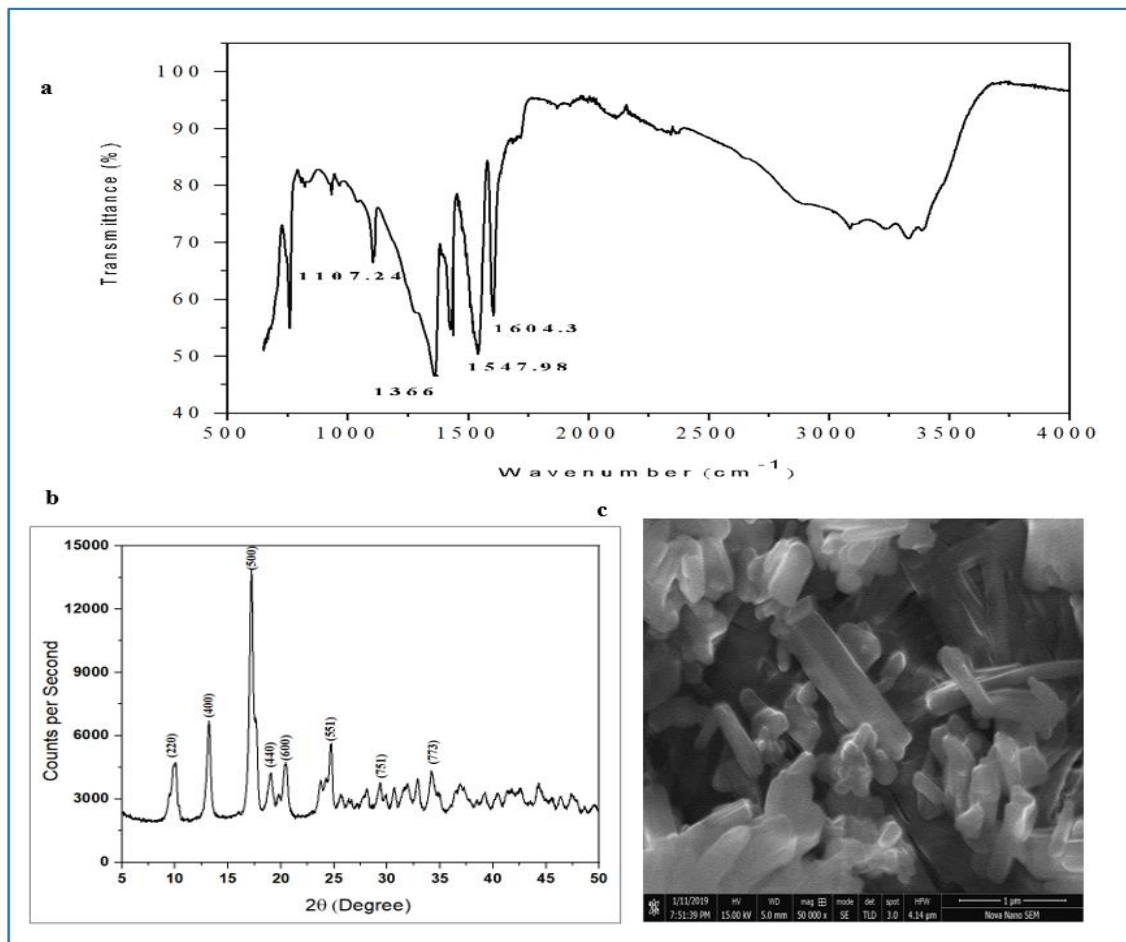
Fig. 3:   FTIR spectrum **a** simulated powder XRD pattern **b** scanning electron micrograph at 1μm resolution **c** for [Pr(BTC)(H$_2$O)$_6$] MOF.

*Characterization of MMMs FTIR studies*

The neat Matrimid®5218 polymer membrane's important and characteristic bands appeared at 1788 and 1723 cm$^{-1}$ that were assigned to be the symmetric and asymmetric stretch for the C=O group on that order. For MMMs, the C=O was identified by the appearance of symmetric stretch at 1778 and 1780 cm$^{-1}$ while the same asymmetric stretch appeared with minor shifting at 1715 and 1711 and 1717 cm$^{-1}$ for 10 wt.% 20 and 30 wt.% MMMs correspondingly. Characteristic imide group could be identified A sharp absorption band was noted for pure Matrimid®5218 membrane at 1361 cm$^{-1}$ for C-N stretch of five member ring of Matrimid®5218. MMMs with 10 and 20 and 30 wt.% loading of MOF showed slight shifting for this absorption band *viz.* 1357, 1364 and 1358 cm$^{-1}$. The stretching vibrations of aromatic double bond appeared at 1510-1512 and 1614, 1547 and 1604 cm$^{-1}$. While the imidic group of Matrimid was shown at 1676 cm$^{-1}$ for pure Matrimid membrane and for the MMM with 30 wt.% loading of MOF, while for MMMs embedded with 10 and 20 wt.% concentration of MOF, imidic group was shown at 1671 and 1612 cm$^{-1}$ (Fig. 4a-4c). Screenshot of 30 wt. % MMM (Fig. 4d) expresses flexible nature of the MMMs.

*Powder XRD studies*

The PXRD patterns of the MMMs fabricated by loading with different weight percentages are shown in Fig. 5 that illustrated the presence of single phase entities all through the fabricated MMMs. The high intensity diffractogram at 2*θ* value of 16° in the pristine Matrimid was shown to be weakened in the resulting MMMs as the primary structure of Matrimid was disrupted [63]. Different intensities of diffractograms of the MMMs indicated the incorporation of different amounts of the additive. While the addition of inorganic additive in the Matrimid matrix did not affect their crystallinity after making a part of the hybrid or MMM.
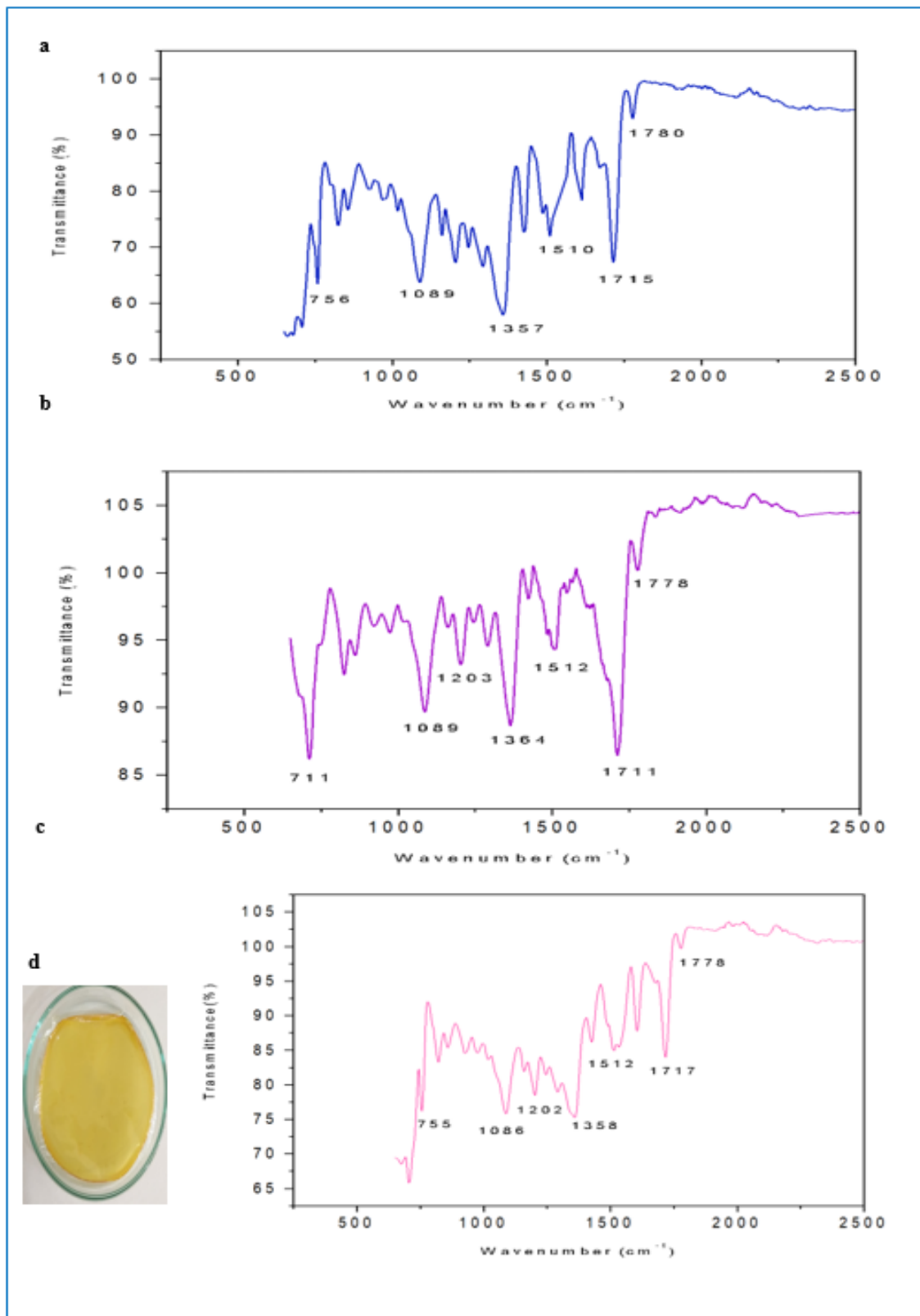
Fig. 4:    FTIR spectra of 10 **a**, 20 **b** 30 wt. % **c** (Pr(BTC)(H$_2$O)$_6$)-Matrimid® MMMs and screenshot **d** of 30 wt.% MMM.
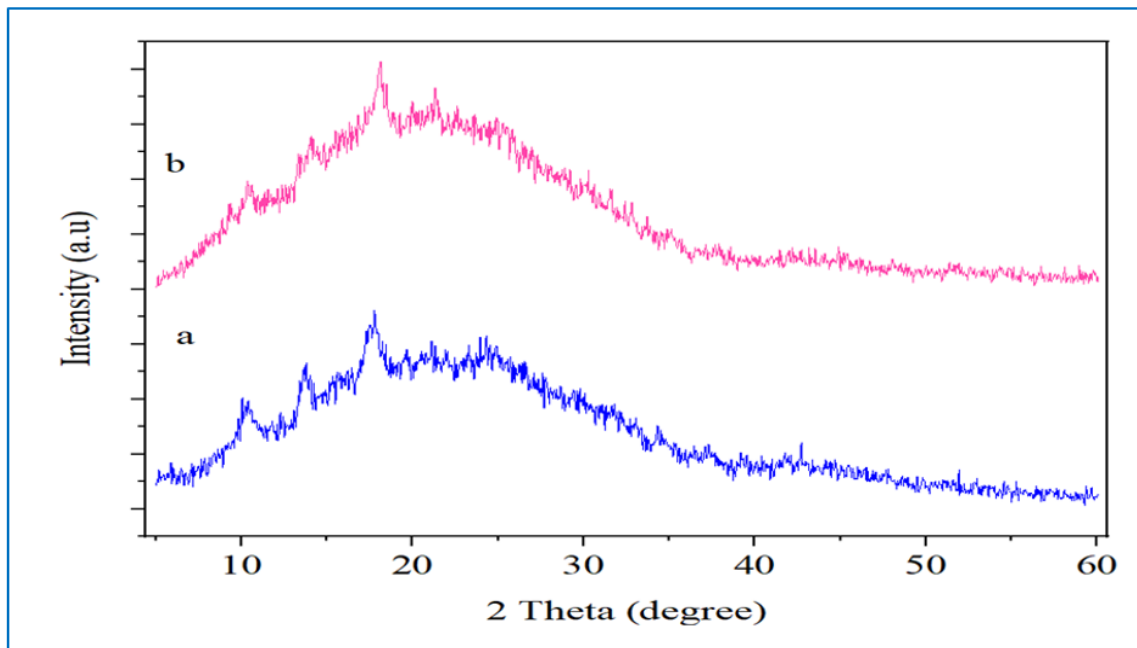
Fig. 5:    Powder XRD patterns of MMMs with 10 wt.% **a** and **b** 30 wt. % MOF.

*TGA studies*

The TGA thermograms and DSC for the MMMs are given in Fig. 6a-6c. There appeared an 8 % weight loss, for MMM, embedded with 10 wt.% concentration of the MOF, at almost 220°C due to solvent molecules loss while a 15.5 % weight loss was observed due to stability loss of the Matrimid® at temperature range between 550-670°C. The polymer was observed to be stable up to 500°C. The first stage of weight loss in MMM with 20 wt.% concentration of the MOF was recorded to be 4 % weight at about 260°C due to the solvent removal and a 25 % weight loss was recorded in the next stage at about 540-770°C. The polymer was found to be stable at up to 500°C after which decomposition started at 540°C. For MMM with 30 wt.% loading, again 5 % weight loss was recorded at about 540-570°C and a 4 % weight loss was recorded for the next stage at 570-650°C. A 10 % weight loss was observed at temperature 800-1000°C. The membrane was observed to be stable up to 500°C afterwards decomposition was started that lasted up to 1000°C.

Thermogravimetric analysis was used to determine percentage loading of MOF particles in MMMs. The Matrimid is stable at higher temperature. The polymer and MOF were decomposed at 1000°C and Pr residue was obtained that was oxidized to $Pr_2O_3$. This residue was used to back calculate the percent MOF loading in MMMs that was 7.7 for 10 wt.% MMM, 17.9 for 20 wt.% and 25.6 for 30 wt.%

MMM. The obtained residual values have shown the increase in amount of Pr with increased MOF loading.

In DSC graph for 10 wt.% MOF containing MMM an endothermic peak appeared at almost 550°C, another small endothermic peak appeared at almost 740°C. The DSC graph for the 20 wt.% MMM exhibited an exothermic peak at about 580°C, while for the 30 wt.% MMM an exothermic peak appeared at 570°C.

*SEM studies*

The MMM having 10 wt.% concentration of the MOF was selected to have an insight into its topological features. The $[Pr(BTC)(H_2O)_6]$ MOF was observed to be well dispersed within the Matrimid matrix yet, with slightly heterogeneous distribution while the SEM images as displayed in Fig. 7a &7b with two different resolutions reveal both phases to be distinct throughout. The SEM images of the MMM incorporating 10 wt.% loading was obtained. While very slight agglomeration was observed in the film which indicated that adequate filler-polymer interactions were still present. However, these agglomerations can further be avoided if the MOF crystals are grinded to more fine powder, protected from moisture exposure, subjected to further dryness and sonication time is increased. The casted membrane modules were sufficiently flexible so as to offer ease of handling. Additionally, better MOF-polymer interactions were observed due to the hybrid nature of the MOF.
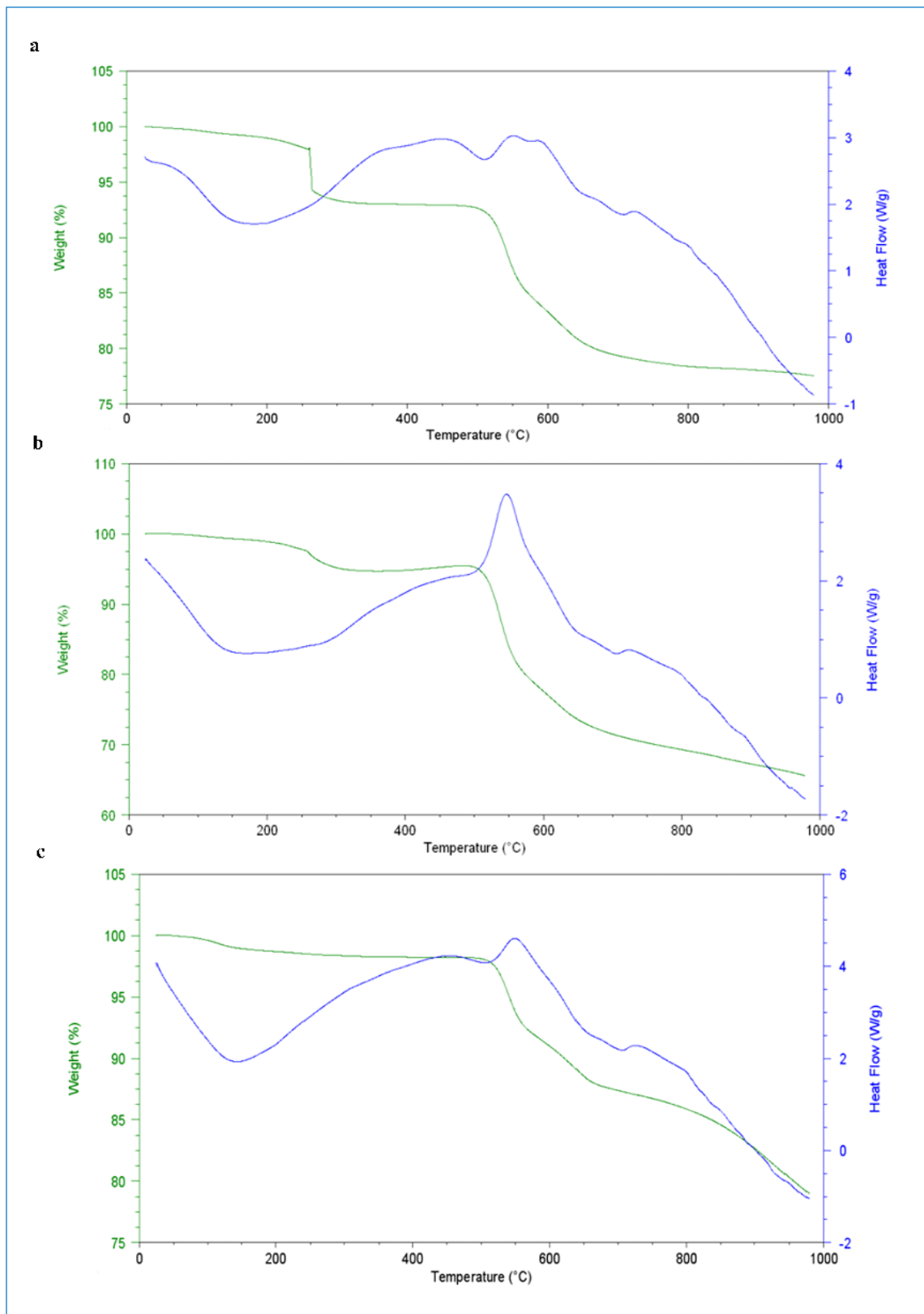
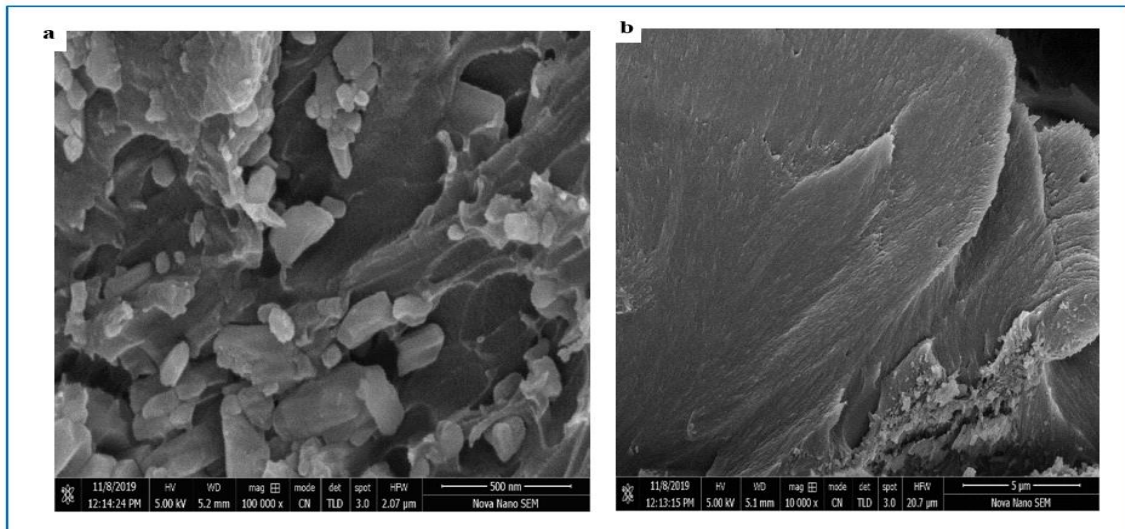Fig. 6:    Thermograms and DSC for 10 **a** 20 **b** and 30 **c** wt.% MMM.

Fig. 7: SEM micrographs of MMM with 10 wt.% loading at 500 nm **a** and 5 μm **b** resolution

*Surface area measurements*

The BET surface area measurements were performed using $N_2$ at 77K and the surface area was found to be 112.450 m²/g. Pore volume was evaluated to be 0.126 cm$^3$/g and the pore width was calculated to be 4.093 nm. The obtained surface area was found to be higher than the previously published results for isostructural [Ce(BTC)(H$_2$O)$_6$] MOF [61] that possessed tunable morphologies [64].

**Conclusion**

Present study deals with fabrication of Matrimid®5218 based mixed matrix membranes (MMMs) by using three weight loadings (10, 20 and 30 wt. %) of nanoporous1D [Pr(BTC)(H$_2$O)$_6$] metal organic framework (MOF). The FTIR spectrophotometric analysis indicated the bonding of lanthanide metal ion with the linker and thus formation of the MOF, and further revealed that the structure of MOF remained sustained after incorporation into the Matrimid matrix. PXRD analysis revealed purity and crystallinity of the MOF while the PXRD results for the MMMs indicated that crystallinity of the MOF remained unaffected after fabrication of the MMMs. The BET surface area of the MOF was also obtained that indicated its permanent porosity. The characterization of the series of novel [Pr(BTC)(H$_2$O)$_6$]/Matrimid-MMMs indicated that these MMMs might be a suitable choice for evaluation of their gas permeation performances particularly the one with higher filler concentration and for the $CO_2$ and $CH_4$ gas pair or some other gases after tuning the filler pore via fabrication with suitable functionality. The filler used may then become a molecular sieving material and the differences in molecular sizes of gases may then will cause selective separation of the gases from their mixture through these MMMs. Selection of good filler-polymer pair results in improved gas separation performances. Their characterization further indicated these MMMs to be defect free in nature and thus a good selection of the polymer-filler pair. The Scanning electron microscopy (SEM) images gave an indication of the formation of the MOF in same morphology as it is previously reported. Additionally, nice distribution and well adherence of the additive particles throughout the Matrimid matrix was observed while the interfacial voids were visibly absent. The MOF and the MMMs were thermally stable and crystallinity of MOF particles remained intact after dispersion into polymer matrix. The MMM with maximum concentration (30 wt. % concentration) of additive might be ascertained to be the better amongst the remaining two MMMs and over the bare Matrimid module too as the said module contains higher amount of filler. Thus these results argue upon the encouragement to test the expected commercial usefulness of the designed MMMs and these MMMs can be proved as potential candidates in the field of gas separation after suitable modification of the filler.

*Chemie, Julius-Maximilians-Universität Würzburg for performing PXRD of the MOF.*

## References

1. W. Zheng, R. Ding, K. Yang, Y. Dai, X. Yan and G. He, ZIF-8 nanoparticles with tunable size for enhanced $CO_2$ capture of Pebax based MMMs, *Sep. Purif. Technol.*, **214**, 111 (2019).

2. M. Babar, M. A. Bustam, A. Ali, A. S. Maulud, U. Shafiq, A. Mukhtar, S. N. Shah, K. Maqsood, N. Mellon and A. M. Shariff, Thermodynamic data for cryogenic carbon dioxide capture from natural gas: A Review, *Cryogenics*, **102**, 85 (2019).

3. N. Tara, Z. Shamair, N. Habib, M. Craven, M. R. Bilad, M. Usman, X. Tu and A. L. Khan, Simultaneous increase in $CO_2$ permeability and selectivity by BIT-72 and modified BIT-72 based mixed matrix membranes, *Chem. Eng. Res. Design*, **178**, 137 (2022).

4. C. Gough, S. Mander and S. Haszeldine, A roadmap for carbon capture and storage in the UK, *Int. J. Greenh. Gas Control*, **4**, 1 (2010).

5. S. Saqib, S. Rafiq, N. Muhammad, A. L. Khan, A. Mukhtar, N. B. Mellon, Z. Man, M. H. Nawaz, F. Jamil and N. M. Ahmad, Perylene based novel mixed matrix membranes with enhanced selective pure and mixed gases ($CO_2$, $CH_4$, and $N_2$) separation, *J. Nat. Gas Sci. Eng.*, **73**, 103072 (2020).

6. V. M. Rangaraj, M. A. Wahab, K. S. K. Reddy, G. Kakosimos, O. Abdalla, E. P. Favvas, D. Reinalda, F. Geuzebroek, A. Abdala and G. N. Karanikolos, Metal organic framework-based mixed matrix membranes for carbon dioxide separation: Recent advances and future directions, *Front. Chem.*, **8**, 534 (2020).

7. R. K. Abdulrahman and I. M. Sebastine, Natural gas sweetening process simulation and optimization: a case study of khurmala field in iraqi kurdistan region, *J. Nat. Gas Sci. Eng.*, **14**, 116 (2013).

8. S. Moioli, L. A. Pellegrini, P. Vergani and F. Brignolit, Study of the robustness of a low-temperature dual-pressure process for removal of $CO_2$ from natural gas, *Front. Chem. Sci. Eng.*, **12**, 209 (2018).

9. M. S. Shafeeyan, W. M. Daud, A. W. A. Shamiri and N. Aghamohammadi, Modeling of carbon dioxide adsorption onto ammonia-modified activated carbon: Kinetic analysis and breakthrough behavior, *Energy & Fuels*, **29**, 6565 (2015).

10. A. Idris, Z. Man, A. S. Maulud, H. A. Mannan and A. Shafie, Effect of silane coupling agents on

11. properties and performance of polycarbonate/silica MMMs, *Polym. Test.*, **73**, 159 (2019).

12. B. H. Monjezi, B. Sapotta, S. Moulai, J. Zhang, R. Oestreich, B. P. Ladewig, K. Müller-Buschbaum, C. Janiak, T. Hashem and A. Knebel, Metal-organic framework MIL-68(In)-$NH_2$ on the membrane test bench for dye removal and carbon capture. *Chemie Ingenieur Technik*, **94**, 135 (2022).

13. S. Hussain, M. H. Wadgama, A. L. Khan, M. Yasin and F. H. Akhtar, Upcycling Poly(ethylene terephthalate) by Fabricating Membranes for Desalination, *ACS Sustainable Chem. Eng.*, **11**, 726 (2023).

14. G. Pilatos, E. C. Vermisoglou, G. E. Romanos, G. N. Karanikolos, N. Boukos, V. Likodimos and N. K. Kenellopoulos, A closer look inside nanotubes: pore structure evaluation of anodized alumina templated carbon nanotube membranes through adsorption and permeability studies, *Adv. Funct. Mater.*, **20**, 2500 (2010).

15. E. P. Favvas and S. K. Papageorgiou, Polyaniline: A promising precursor material for membrane technology applications, Hauppauge, NY: Nova Science Publishers, **2013**, (2013).

16. M. Pera-Titus, Porous inorganic membranes for $CO_2$ capture: present and prospects, *Chem. Rev.*, **114**, 1413 (2014).

17. J. A. Stoeger, C. M. Veziri, M. Palomino, A. Corma, N. K. Kanellopoulos, M. Tsapatsis and G. N. Karanicolos, On stability and performance of highly *c*-oriented columnar $AlPO_4$-5 and CoAPO-5 membranes, *Micro. Mesoporous Mater.*, **147**, 286 (2012).

18. A. A. Alomair, S. M. Al-Jubouri and S. M. Holmes, A novel approach to fabricate zeolite membranes for pervaporation processes, *J. Mater. Chem. A.*, **3**, 9799 (2015).

19. M. A. Abdulhameed, M. H. D. Othman, A. F. Ismail, T. Matsuura, Z. Harunm, M. A. Rahman and S. K. Hubadillah, Carbon dioxide capture using a superhydrophobic ceramic hollow fiber membrane for gas-liquid contacting process, *J. Clean. Prod.*, **140**, 1731 (2017).

20. Z. Hu, Z. Kang, Y. Qian, Y. Peng, X. Wang, C. Chi and D. Zhao, Mixed matrix membranes containing UiO-66(Hf)-$(OH)_2$ Metal organic framework nanoparticles for efficient $H_2/CO_2$ separation, *Ind. Eng. Chem. Res.*, **55**, 7933 (2016).

21. M. W. Anjum, F. Vermoortele, A. L. Khan, B. Bueken, DE De Vos and I. F. J. Vankelecom, Modulated UiO-66 based mixed matrix membranes for $CO_2$ separation, *ACS Appl. Mater. & Interfaces*, **7**, 25193 (2015).

22. M. Mubashir, Y. F. Yeong, T. L. Chew and K. K. Lau, Issues and current trend of hollow fiber mixed

matrix membranes for $CO_2$ separation from $N_2$ and $CH_4$, *Chem. Eng. Technol.*, **41**, 235 (2017).

22. L. M. Robeson, Correlation of separation factor versus permeability for polymeric membranes, *J. Membrane Sci.*, **62**, 165 (1991).

23. L. M. Robeson, The upper bound revisited, *J. Membrane Sci.*, **320**, 390 (2008).

24. J. Zhang, J. A. Schott, Y. Li, W. Zhan, S. M. Mahurin, K. Nelson, X. G. Sun, M. P. Paranthaman and S. Dai, Membrane-based gas separation accelerated by hollow nanosphere architectures, *Adv. Mater.*, **29**, 1603797 (2017).

25. M. Rezakazemi, A. E. Amooghin, M. M. Montazer-Rahmati, A. F. Ismail and T. Matsuura, State-of-the-art membrane based $CO_2$ separation using mixed matrix membranes (MMMs): An overview on current status and future directions, *Prog. Polym. Sci.*, **39**, 817 (2014).

26. B. Zornoza, C. Téllez, J. Coronas, J. Gascon and F. Kapteijn, Metal organic framework based mixed matrix membranes: an increasingly important field of research with a large application potential, *Micro. Mesoporous Mater.*, **166**, 67 (2013).

27. M. G. Miricioiu, C. Iacob, G. Nechifor and V.-C. Niculescu, High selective mixed matrix membranes based on mesoporous MCM-41 and MCM-41-$NH_2$ particles in polysulfone matrix, *Front. Chem.*, **7**, article 332 (2019).

28. P. Moradihamedani, N. A. Ibrahim, W. M. Z. W. Yunus and N. A. Yusof, Preparation and characterization of symmetric and asymmetric pure polysulfone membranes for $CO_2$ and $CH_4$ separation, *Polym. Eng. and Sci.,* **54**, 1686 (2014).

29. M. R. A. Hamid and H. K. Jeong, Recent advances on mixed-matrix membranes for gas separation: Opportunities and engineering challenges, *Korean J. Chem. Eng.*, **35**, 1577 (2018).

30. M. J. C. Ordoñez, K. J. B. Balkus Jr, J. P. Ferraris and I. H. Musselman, Molecular sieving realized with ZIF-8/Matrimid® mixed-matrix membranes, *J. Membrane Sci.*, **361**, 28 (2010).

31. Q. Song, S. K. Nataraj, M. V. Roussenova, J. C. Tan, D. J. Hughes, W. Li, P. Bourgoin, M. A. Alam, A. K. Cheetham, S. A. Al-Muhtaseb and E. Sivaniah, Zeolitic imidazolate framework (ZIF-8) based polymer nanocomposite membranes for gas separation, *Energy & Environ. Sci.*, **5**, 8359 (2012).

32. S. U. Hassan, S. Shafique, B. A. Palvasha, M. H. Saeed, S. A. R. Naqvi, S. Nadeem, S. Irfan, T. Akhter, A. L. Khan, M. S. Nazir, M. Hussain and Y.-K. Park, Photocatalytic degradation of industrial dye using hybrid filler impregnated poly-sulfone membrane and optimizing the catalytic performance using Box-Behnken design, *Chemosphere*, **313**, 137418 (2023).

33. A. Alkhouzaam and H. Qiblawey, Novel polysulfone ultrafiltration membranes incorporating polydopamine functionalized graphene oxide with enhanced flux and fouling resistance, *J. Membrane. Sci.*, **620**, 11890 (2021).

34. S. H. Ding, T. Y. S. Ng, T. L. Chew, P. C. Oh, A. L. Ahmad and C.-D. Ho, Evaluation of the properties, gas permeability, and selectivity of mixed matrix membrane based on polysulfone polymer matrix incorporated with KIT-6 silica, *Polymers*, **11**, 1732 (2019).

35. S. Kim and E. Marand, High permeability nano-composite membranes based on mesoporous MCM-41 nanoparticles in a polysulfone matrix, *Micro. Mesoporous Mater.*, **114**, 129 (2008).

36. A. Jomekian, M. Pakizeh, S. Mansoori, M. Poorafshari, M. Hemmati, and D. P. Ataee, Gas transport behavior of novel modified MCM-48/polysulfone mixed matrix membrane coated by PDMS, *J. Membrane. Sci. Technol.*, **1**, 1 (2011).

37. P. Falcaro, R. Ricco, C. M. Doherty, K. Liang, A. J. Hill, and M. J. Styles, MOF positioning technology and device fabrication, *Chem. Soc. Rev.*, **43**, 5513 (2014).

38. M. Safaei, M. M. Foroughi, N. Ebrahimpoor, S. Jahani, A. Omidi, and M. Khatami, A review on metal-organic frameworks: Synthesis and applications, TrAC *Trends Anal. Chem.*, **118**, 401 (2019).

39. X. Guo, H. Huang, Y. Ban, Q. Yang, Y. Xiao, Y. Li, W. Yang and C. Zhong, Mixed matrix membranes incorporated with amine-functionalized titanium-based metal-organic framework for $CO_2$/$CH_4$ separation, *J. Membrane Sci.*, **478**, 130 (2015).

40. A. L. Khan, C. Klaysom, A. Gahlaut and I. F. J. Vankelecom, Polysulfone acrylate-membranes containing functionalized mesoporous MCM-41 for $CO_2$ separation, *J. Membrane Sci.*, **436**, 145 (2013).

41. S. Sorribas, B. Zornoza, C. Téllez and J. Coronas, Mixed matrix membranes comprising silica- (ZIF-8) core-shell spheres with ordered meso-microporosity for natural- and bio-gas upgrading, *J. Membrane Sci.*, **452**, 184 (2014).

42. B. Zornoza, B. Seoane, J. M. Zamaro, C. Téllez and J. Coronas, Combination of MOFs and zeolites for mixed-matrix membranes, *Chem. Phys. Chem.*, **12**, 2781 (2011).

43. B. Zornoza, A. Martinez-Joaristi, P. Serra-Crespo, C. Tellez, J. Coronas, J. Gascon and F. Kapteijn, Functionalized flexible MOFs as fillers in mixed matrix membranes for highly selective separation of $CO_2$ from $CH_4$ at elevated pressures, *Chem. Comm.*, **47**, 9522 (2011).

44. M. T. Khalid, T. Anjum, A. L. Khan, F. Rehman, M. Aslam, M. A. Gilani, F. H. Akhtar, M. Lee, I. S. Chang and M. Yasin, Task-specific polymeric

membranes to achieve high gas-liquid mass transfer, *Chemospere*, **313**, 137603 (2023).

45. A. Car, C. Stropnik and K.-V. Peinemann, Hybrid membrane materials with different metal-organic frameworks (MOFs) for gas separation, *Desalination*, **200**, 424 (2006).

46. T. Rodenas, M. van Dalen, P. Serra-Crespo, F. Kapteijn and J. Gascon, Mixed matrix membranes based on $NH_2$-functionalized MIL-Type MOFs: influence of structural and operational parameters on the $CO_2/CH_4$ separation performance, *Micro. Mesoporous Mater.*, **192**, 35 (2014).

47. F. Dorosti, M. Omidkhah and R. Abedini, Fabrication and characterization of Matrimid/MIL-53 mixed matrix membrane for $CO_2/CH_4$ separation, *Chem. Eng. Res. Design*, **92**, 2439 (2014).

48. C. Liu, B. McCulloch, S. T. Wilson, A. I. Benin and M. E. Schott., Metal organic framework-polymer mixed matrix membranes, US Patent-7637983B1 (2009).

49. H. Wu, X. Q. Li, Y. F. Li, S. F. Wang, R. L. Guo, Z. Y. Jiang, C. Wu, Q. P. Xin and X. Lu, Facilitated transport mixed matrix membranes incorporated with amine functionalized MCM-41 for enhanced gas separation properties, *J. Membrane Sci.*, **465**, 78 (2014).

50. T. L. Chew, S. H. Ding, P. C. Oh, A. L. Ahmad and C.-D. Ho, Functionalized KIT-6/polysulfone mixed matrix membranes for enhanced $CO_2/CH_4$ gas separation, *Polymers*, **12**, 2312 (2020).

51. Z. Tahir, M. Aslam, M. A. Gilani, M. R. Bilad, M. W. Anjum, L.-P. Zhu, A. L. Khan, $-SO_3H$ functionalized UiO-66 nanocrystals in Polysulfone based mixed matrix membranes: Synthesis and application for efficient $CO_2$ capture, *Sep. and Purif. Technol.*, **224**, 524 (2019).

52. J. Dechnik, F. Mühlbach, D. Dietrich, T. Wehner, M. Gutmann, T. Lühmann, L. Meinel, C. Janiak, K. Müller-Buschbaum, Luminescent Metal-Organic Framework Mixed-Matrix Membranes from Lanthanide Metal-Organic Frameworks in Polysulfone and Matrimid, *Eur. J. Inorg. Chem.*, **2016**, 4408 (2016).

53. J. M. Stangl, D. Dietrich, A. E. Sedykh, C. Janiak, K. Müller-Buschbaum, Luminescent MOF polymer mixed matrix membranes for humidity sensing in real status analysis, *J. Mater. Chem. C.*, **6**, 9248 (2018).

54. J. Luo, H. Xu, Y. Liu, Y. Zhao, L. L. Daemen, C. Brown, T. T. Timofeeva, S. Ma and H.-C. Zhou, Hydrogen adsorption in a highly stable porous rare-earth metalorganic framework: Sorption properties and neutron diffraction studies, *J. Am. Chem. Soc.*, **130**, 9626 (2008).

55. F. Wang, Y. Han, C. S. Lim, Y. H. Lu, J. Wang, J. Xu, H. Y. Chen, C. Zhang, M. H. Hong and X. G. Liu, Simultaneous phase and size control of up-conversion nanocrystals through lanthanide doping, *Nature*, **463**, 1061 (2010).

56. K. Liu, Y. Zheng, G. Jia, M. Yang, Y. Huang and H. You, Facile synthesis of hierarchically superstructured praseodymium benzenetricarboxylate with controllable morphologies, *Cryst. Eng. Comm.*, **13**, 452 (2011).

57. X. D. Guo, G. S. Zhu, Z. Y. Li, F. X. Sun, Z. H. Yang and S. L. Qiu, A lanthanide metal-organic framework with high thermal stability and available Lewis-acid metal sites, *Chem. Comm.*, **30**, 3172 (2006).

58. R. Łyszczek, Thermal and spectroscopic investigations of new lanthanide complexes with 1,2,4-benzenetricarboxylic acid, *J. Therm. Anal. Calorim.*, **90**, 533 (2007).

59. R. Łyszczek. Z. Rzączyńska, A. Kula and A. Gładysz-Płaska, A Thermal and luminescence characterization of lanthanide 2,6-naphthalenedicarboxylates series, *J. Anal Appl. Pyrolysis*, **92**, 347 (2011).

60. Y.-H., Wen, J.-K. Cheng, Y.-L. Feng, J. Zhang, Z.-J. Li and Y.-G. Yao, Synthesis and crystal structure of $[La(BTC)(H_2O)_6]_n$, *Chinese. J. Struct. Chem.*, **24**, 1440 (2005).

61. S. Maiti, A. Pramanik, S. Mahanty, Extraordinarily high pseudocapacitance of metal organic framework derived nanostructured cerium oxide, *Chem. Comm. RSC Publishing.*, **50**, 11717 (2014).

62. F. Wang, K. Deng, G. Wu, H. Liao, H. Liao, L. Zhang, S. Lan, J. Zhang, X. Song and L. Wen, Facile and large-scale syntheses of nanocrystal rare earth metal-organic frameworks at room temperature and their photoluminescence properties, *J. of Inorg. Organomet. Polym and Mater.*, **22**, 680 (2012).

63. J. Ahmad and M.-B. Hägg, Development of matrimid/zeolite 4A mixed matrix membranes using low boiling point solvent, *Sep. Purif. Technol.*, **115**, 190 (2013).

64. K. Liu, H. You, G. Jia, Y. Zheng, Y. Huang, Y. Song, M. Yang, L. Zhang and H. Zhang, Hierarchically nanostructured coordination polymer: Facile and rapid fabrication and tunable morphologies, *Crys Growth Design.*, **10**, 790 (2010).